iScience

CellPress
OPEN ACCESS

Article

Anisotropic porous designed polymer coatings for high-performance passive all-day radiative cooling

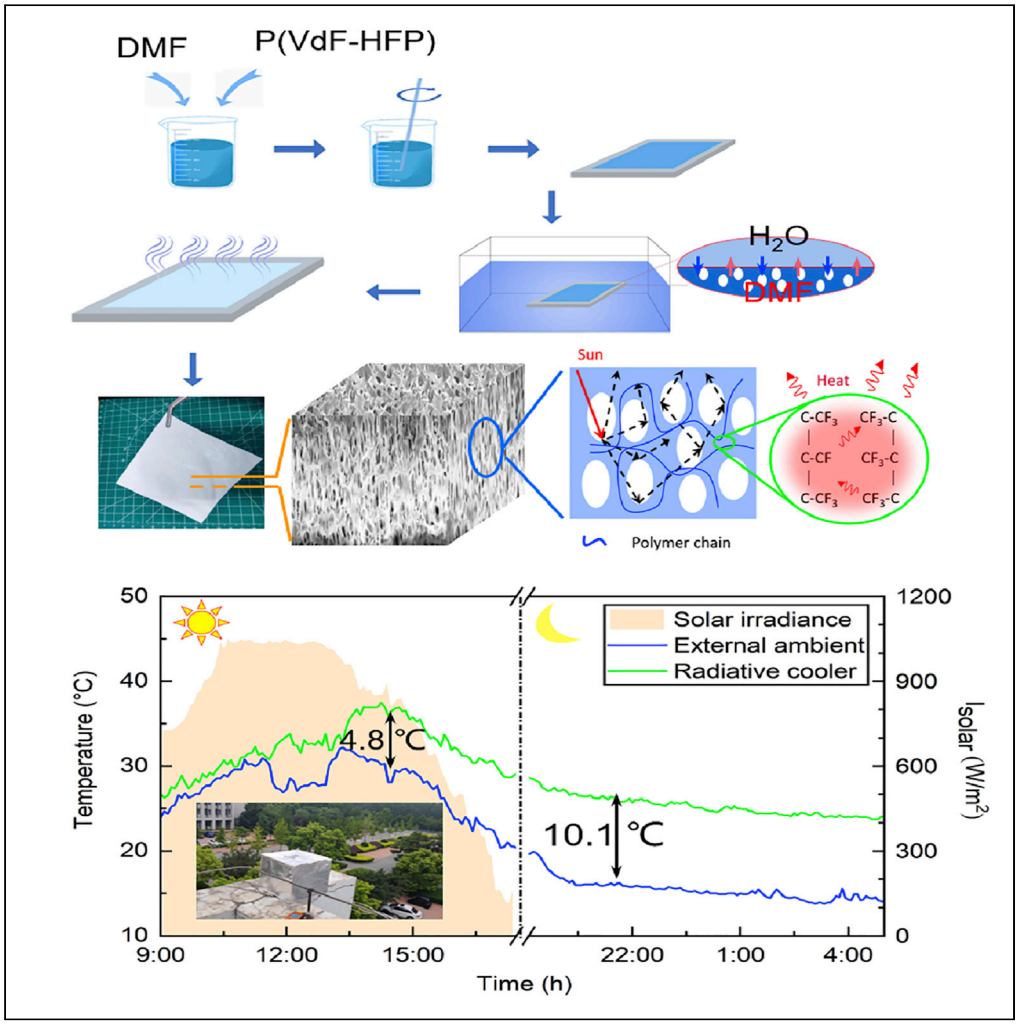

Jiliang Zhu, Zhiqiang An, Anxun Zhang, Yike Du, Xuan Zhou, Yizhao Geng, Guifeng Chen

jlzhu@hebut.edu.cn

Highlights

Anisotropic porous designed polymer coatings for passive all-day radiative cooling

Dissolution and diffusion of the solvent and non-solvent cause phase separation

Adjustment of pore shape and size of polymer coating by phase separation process

High cooling and power generation efficiency achieved with anisotropic coatings

Zhu et al., iScience 25, 104126
April 15, 2022
https://doi.org/10.1016/j.isci.2022.104126

iScience

CellPress
OPEN ACCESS

Article

Anisotropic porous designed polymer coatings for high-performance passive all-day radiative cooling

Jiliang Zhu,[1,3,*] Zhiqiang An,[1] Anxun Zhang,[1] Yike Du,[1] Xuan Zhou,[1] Yizhao Geng,[1] and Guifeng Chen[2]

SUMMARY

Porous polymer radiative cooling coatings (PPCs) have attracted attention due to their ability of drawing and radiating heat from a hot object into the outer space, without any energy consumption. However, high performance of PPCs has yet to be achieved and the large-scale production of radiative cooling technology is still facing high cost and complex manufacturing constraints. Here, we propose a simple, inexpensive, scalable approach to fabricate anisotropic $(P(VdF\text{-}HFP))_{ap}$ PPCs (TPCs) by dissolution and diffusion between solvent and non-solvent-induced phase separation. By adjusting the porosity, pore size, and geometry, a sub-ambient temperature drop of ~6.3°C in daytime and 10.1°C in night-time was achieved under a solar reflectance of 0.92 and an atmospheric window emittance of 0.96. A thermoelectric generator with an output voltage of almost zero reached 7 V/m^2 after coating with TPCs. This could provide a convenient, economical, and environment-friendly way for PPCs materials toward efficient cooling and power generations.

INTRODUCTION

Cooling plays more and more important roles in people's daily life. Compressing gas and fluid (gas or liquid) are commonly used for cooling with obvious shortcomings like water resources consumption, electric energy consumption, ozone-depleting, and greenhouse gas emissions. It is particularly important to find a novel environmentally friendly method for cooling (Gentle and Smith, 2015; Munday, 2019). Passive daytime radiative cooling (PDRC) is one of the best ways to irradiate heat to the cold outer space through atmospheric infrared transparent windows and resist heat absorption of the radiative devices from the sun (Goldstein et al.2017; Zhang et al., 2019; Peng et al., 2018; Zhang et al., 2020; Zhai et al., 2017). Some PDRC technologies have been proposed using nanophotonic structures (Kou et al., 2017; Raman et al., 2014; Kort-Kamp et al., 2018), nanoparticles (Mu et al., 2019; Xia et al., 2019; Leonov et al., 2007), and pores (Li et al., 2019; Mandal et al., 2018; Kim et al., 2020; Li et al., 2021; Liu et al., 2019) to enhance the radiation intensity of the corresponding atmospheric infrared transparent windows and inhibit the solar absorbance via reflecting sunlight. To this end, a simple, inexpensive and scalable hierarchically porous coating of ~6°C sub-ambient temperature drop has been obtained by a simple, inexpensive, and scalable phase-inversion-based method. The rapid evaporation of the volatile acetone causes the Poly (vinylidene fluoride-co-hexafluoropropene) (P(VdF-HFP)) to phase-separate from the water, which forms spherical micro- and nanodroplets (Mandal et al., 2018). A variety of polymer cooling materials have been made using phase inversion method (Mandal et al., 2018; Xiang et al., 2021; Wang et al., 2021), thermally induced phase separation (TIPS) method (Yang et al., 2020), electrostatic spinning (Li et al., 2021; Wang et al., 2020), and combined with aerogel (Leroy et al., 2019; Zhou et al., 2021). While these designs are effective, the large-scale production of radiative cooling technology still faces with high cost and complex manufacturing constraints. Therefore, design and fabrication of novel energy saving and environment-friendly PDRC systems need in-depth study.

In this work, non-solvent-induced phase separation (NIPS), a simple, inexpensive, and scalable method commonly used to make diaphragm and ultrafiltration membrane (Luque-Alled et al., 2020; Li et al., 2014), is applied to make cooling coatings for daytime passive radiation cooling. The porous polymers start from the preparation of a precursor solution of P(VdF-HFP) (polymer) and water (non-solvent) in dimethylformamide (DMF, solvent). The solubility and diffusivity of the DMF causes the P(VdF-HFP) to phase-separate from the

[1]Department of Applied Physics, Hebei University of Technology, Tianjin 300401, P. R. China

[2]School of Materials Science and Engineering, Hebei University of Technology, Tianjin 300132, P. R. China

[3]Lead contact

*Correspondence: jlzhu@hebut.edu.cn

https://doi.org/10.1016/j.isci.2022.104126

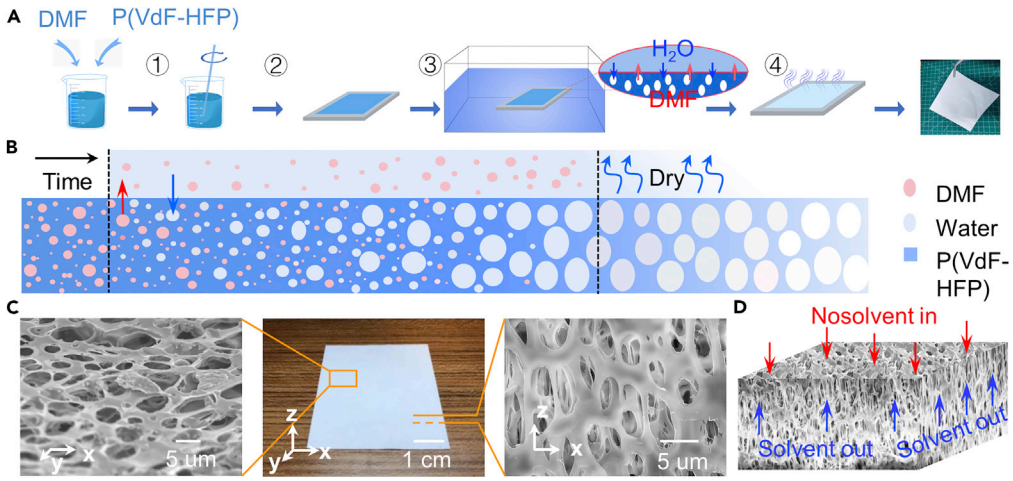

Figure 1. The fabrication of TPC and its SEM images

(A) Schematic diagram of phase separation process in NIPS method. The NIPS method was mainly divided into 4 steps: dissolving, applying, immersing, and drying.

(B)Schematic showing the fabrication porous $P(VdF\text{-}HFP)_{ap}$ coating by NIPS process.

(C) Physical picture of TPCs on the wooden table and its SEM images of top- and cross- section.

(D) Schematic diagram of anisotropic micropore formation.

water, which forms anisotropic microdroplets. The porosity, pore size, and pore geometry can be adjusted by preparation process. This method has advantages of low pollution, low energy consumption, and no complicated instruments in the preparation process. By experiments and theoretical calculations, it was confirmed that the designed and fabricated anisotropic P(VdF-HFP) ($(P(VdF\text{-}HFP))_{ap}$) porous polymer radiative cooling coatings (TPCs) via the NIPS process could achieve high solar reflectance and atmospheric window emittance. When the solar reflectance (R_{solar}) was 0.92 (Normal incidence measurement) and long-wave infrared (LWIR) atmospheric transmission window ($\lambda \sim 8$–13 μm) emittance (ε_{LWIR}) was 0.96 (Normal incidence measurement), an average cooling temperature (ΔT) of 6.3°C in the daytime achieved and the corresponding maximum temperature drop was over 9°C. Strong mechanical strength, good flexibility, and well ductility make TPCs have certain ability to resist the deformation of the structure on the various substrates. Besides cooling, a thermoelectric generator was proposed using the papered TPCs and its output voltage achieved 7 V/m^2. This provides a convenient, economical, and environment-protecting way for the preparation of PDRC materials toward power generations.

RESULTS

Non-solvent-induced phase separation method

In 1963, Loeb and Sourirajan invented the phase inversion membrane production method (Yampolskii, 2012), which made the polymer separation membranes valuable for industrial applications. Thereafter, the phase inversion membrane production has been extensively studied and gradually become the mainstream preparation way for polymer separation membranes. Among the phase inversion approaches, the NIPS has a simpler preparation process and more process variability. NIPS can adjust the structure and performance of the membrane according to the application of the membrane. It has become the main method for preparing microporous membranes (Liu et al., 2013, 2020; Kim et al., 2017). However, there is no report on PDRC so far.

Figure 1A shows the schematic of the production process of TPCs in the NIPS process, which can be divided into four steps. Firstly, the P(VdF-HFP) powder is dissolved in an organic solvent dimethylformamide (DMF). Secondly, a coating is applied onto a clean glass substrate in a certain thickness. Thirdly, they are immersed into condensed water (deionized water) immediately, and the DMF will displace out of polymer precipitates resulting in a porous polymer network. Eventually, loose and porous TPCs are got after drying. The porosity of the TPCs can reach to more than 60%. More importantly, the shape, size, and number of pores can be further controlled by adjusting the process, which are favorable to regulate reflection and radiation for specific applications.

When the polymer solution is immersed into water, the DMF as solvent is continuously exchanged with the outside water (Figure 1B). The content of DMF will be getting lower, while the content of water will be getting higher. Because the solvents have good mutual solubility with water, during the phase transformation process, the solvent and non-solvent produce double diffusion perpendicular to the surface of the coating (Liu et al., 2020). The water is immiscible with the P(VdF-HFP)ap in the system, and small water droplets will merge themselves to form larger pores. We conjectured that the up-down double diffusion process makes the anisotropic micropores whose long axis is perpendicular to the film interface appear in the polymer in the casting solution (Figure 1C). This process is accompanied by the occurrence of phase separation (see Figure S1). After drying, the TPCs with a large number of air pores are formed. In addition, in order to ensure the repeatability of coatings production, some factors also should be paid attention to in the coating production process (See STAR Methods). With the approach, we fabricated a TPC with size of 5 cm * 5 cm and thickness of 400 μm. Its top- and cross-section structures were observed by a scanning electron microscope (SEM), as shown in Figure 1D. From the top-section, it can be seen that the micropores are mostly round pores with the radius of about 4 μm, while the cross section shows oval pores of 4 μm * 7 μm. We define such pores like ellipsoid in the TPCs as anisotropic pores, differing from the isotropic pores that have been reported (Zhai et al., 2017; Mandal et al., 2018). Owing to the anisotropy of the micropore shape in the structure, the coating is anisotropy to the optics. Here, the parameters minor axes (l_x and l_y) and major axes (l_z) are defined to describe the sizes and geometry of the micropores, which usually are $l_x \approx l_y < l_z$. Such anisotropic pores might be conducive to enhancing the R_{solar} and inhibiting the ε_{LWIR}.

Sub-ambient PDRC performances

The PDRC schematic diagram of our TPCs including the backscattering sunlight and emitting thermal radiation is showed in Figure 2A. Figure 2B is the reflection and emittance spectrum of TPCs with effective thickness of 400 μm according to the normalized ASTM G173 Global solar spectrum and the atmosphere's LWIR transparency window. The results demonstrate that our TPC with a porosity of ~64% achieves an R_{solar} of 0.92, which makes the coating to minimize the heat absorbed from the solar. In addition, the TPC has an excellent ε_{LWIR} of 0.96 with a broad bandwidth, which can emit heat to the cold outer space strongly through the atmosphere's LWIR transparency window.

One of the characteristics of our TPC is unique porous structure with size of ~4 μm * 7 μm, which can scatter the sunlight of ultraviolet-visible-near-infrared (UV-Vis-NIR) wavelength. Compared with the circular pores, anisotropic pores increase the scattering probability of light propagating in the thin film due to their shape characteristics, and the anisotropic pores greatly decrease the mean scattering path, which further enhance the scattering of UV-Vis-NIR wavelength. We also get the same conclusions by using simulations with finite-difference time-domain (FDTD) method (Figures 2C, 2D, and S2). The anisotropic pores ($l_y < l_z$) have stronger scattering ability for sunlight than circular pores ($l_y = l_z$). The scattering coefficient of 0.8 um * 1.4 um micropore declined in the near-infrared band, and that of 8 um * 14 um micropore declined in the ultraviolet band. Only the anisotropic pores of 4 um * 7 um can effectively scatter the full wavelength of sunlight of UV-Vis-NIR. In addition, when sunlight passed through the interface between $P(VdF\text{-}HFP)_{ap}$ (high refractive index $n_{P(VdF\text{-}HFP)ap} = 1.4$) and air pore (low refractive index $n_{air} = 1.0$), the high refractive index difference ($n_{P(VdF\text{-}HFP)} - n_{air} = 0.4$) can provide a sharp refractive index change across boundaries between P(VdF-HFP) and air, and come into being the efficient sunlight scattering. All told, the anisotropic pores can achieve an excellent R_{solar} more easily than circular pores with the same size.

As a cooling membrane material, $P(VdF\text{-}HFP)_{ap}$ has two absorption peaks in the atmospheric window (8–13 μm) including F-C-F (symmetric stretching vibration mode, ~1190 cm^{-1}) and $-CF_3$ (1069 cm^{-1}), as shown in Figure 2E. Besides the anisotropic pores, another characteristic is worth noting that two novel absorption peaks in the atmospheric window were observed in our TPCs: the peaks of the amorphous structure (873 cm^{-1}) from HFP and the β-phase structure (842 cm^{-1}) derived from PVdF (Figure 2E) (Bormashenko et al., 2004; Sim et al., 2012; Ulaganathan and Rajendran, 2010). Amazingly, the most common α-phase of the PVdF did not appear at its characteristic peaks (761 cm^{-1} and 986 cm^{-1}). The reason may be that water and DMF are both strongly polar solvents and the double diffusion that occurred during the immersion process changed the arrangement direction of the $-CF_2$ (permanent dipoles). This resulted in that the α-phase was transformed into the β-phase, which might be conducive to radiating heat into the outer space.

The cooling performance of our TPCs has been evaluated by a system consisted of a 30 cm * 30 cm * 30 cm acrylic box filled with polyethylene (PE) foam (Figure 2F). The thickness of each acrylic plate was about

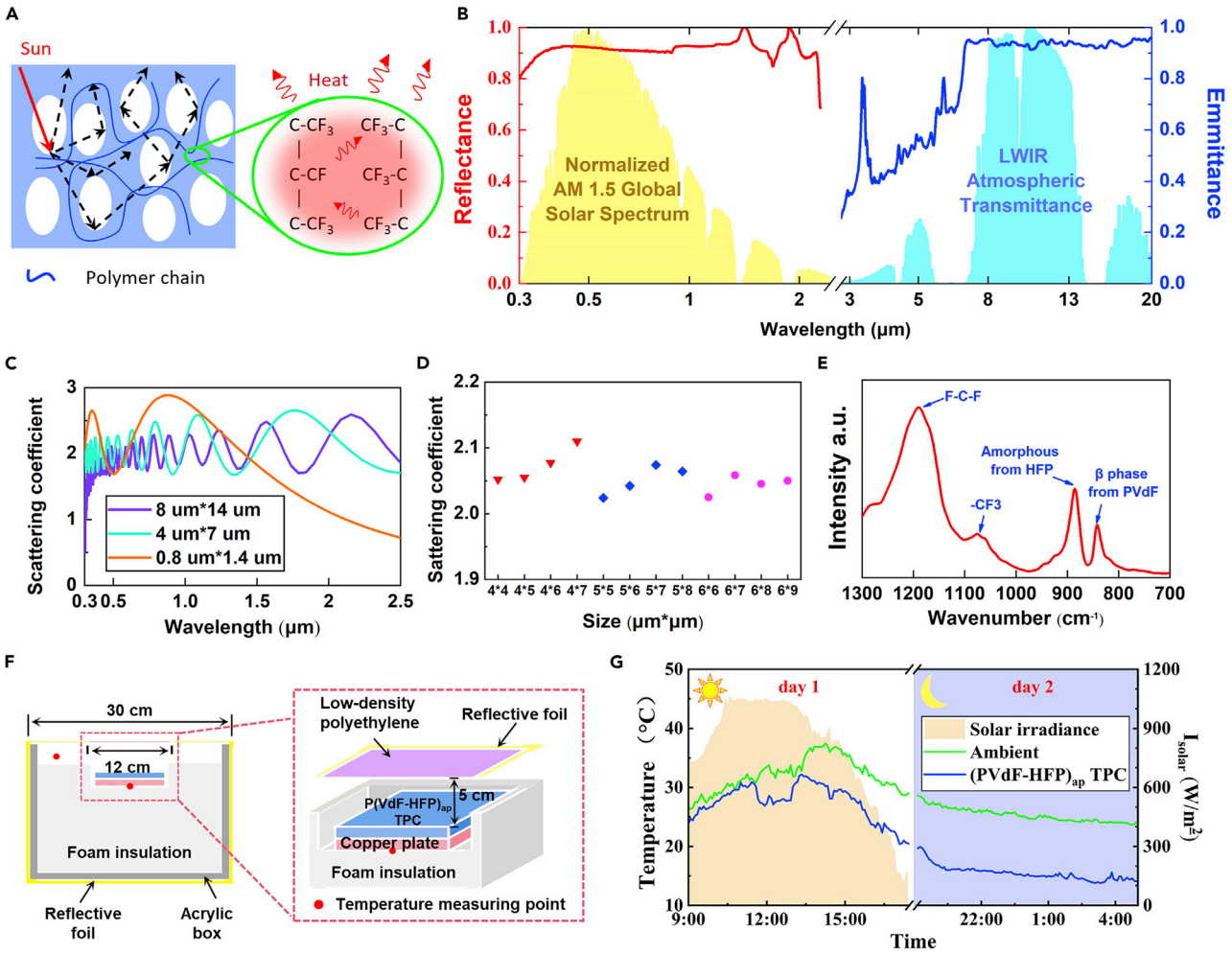

Figure 2. Outdoor test site, equipment, and cooling performances

(A) Schematic of the basic principles of PDRC. The TPCs strongly scatter sunlight through a large number of air micropores, and emit thermal radiation through specific functional groups.

(B) R_{solar} and ε_{LWIR} of the TPC. The yellow and blue background images show the normalized ASTM G173 global solar spectrum and LWIR atmospheric transparency window, respectively. The atmospheric light transmittance was calculated using the atmospheric transmittance calculation software *MODTRAN 4*.

(C and D) The calculated scattering coefficients and scattering efficiency of the TPC with different sizes.

(E) Infrared spectrum within the atmospheric window (8–13 um) of the TPC.

(F and G) Schematic of the setup for testing performance of TPCs under sunlight and detailed solar intensity and temperature data on a clear but windy day in Tianjin. The illustration showed the test site, which was located on the roof of a four-story building in the Hebei University of Technology in Tianjin, China (39.23N, 117.05E).

0.5 cm and the height of the foam was 27 cm. A cuboid pit of 10 cm * 10 cm * 2 cm was dug in the center of the top of the foam, and the copper pieces of 10 cm *10 cm * 1 mm were put into the pit. The TPCs were pasted on the copper sheet with thermally conductive adhesive (thermal conductivity was 12 W/(m^2·K)). Here, the copper sheet was to facilitate the measurement of accurate temperature. The top of the acrylic box was covered with tin foil. There was a 12 cm * 12 cm pore in the center of the tin foil, which was located directly above the foam pit. The square pore in the middle was sealed with a layer of PE plastic wrap to reduce convection heat. This allowed the coating to radiate heat through the window while preventing sunlight from heating the box violently. The temperature of coatings under the copper plate and the ambient air in the shade inside the acrylic box were measured with two calibrated thermocouples of the same K type (range from −50°C to 300°C, accuracy of 0.1°C, relative error of ±1.5%). Solar irradiance, atmosphere temperature, and atmosphere humidity were also measured using a portable meteorological station. The meteorological station's temperature sensors and type K thermocouples were pre-calibrated.

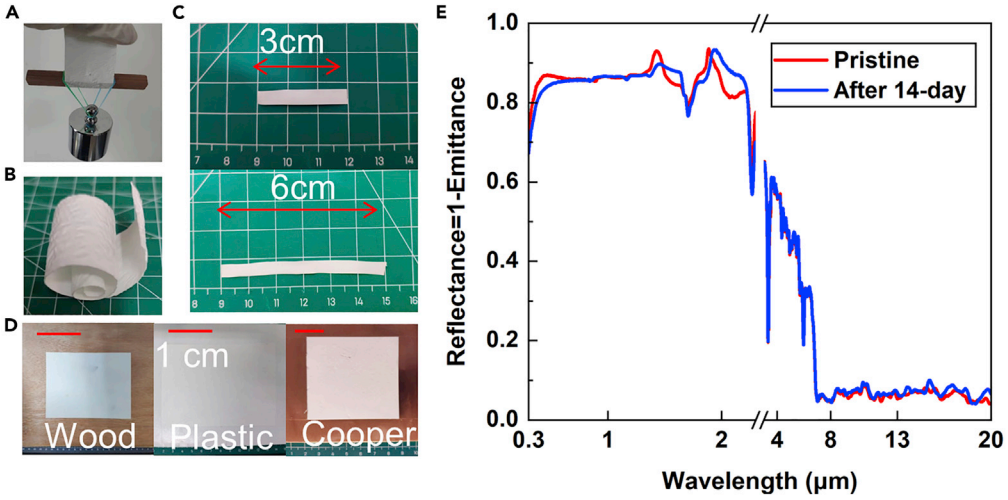

Figure 3. Mechanical strength, flexibility, ductility, and weather resistance of the TPCs

(A) The TPC supported a farmar of 1 kg (3 cm wide and 500 microns thick).

(B) The image of a TPC bent 180 degrees.

(C) The good ductility of TPC, which could be slowly stretched to 6 cm from 3 cm. The thickness reduced after stretching.

(D) Photographs of TPCs made on substrates of wood, plastic, and polished metal.

(E) R_{solar} and ε_{LWIR} curves of TPC before and after 14 days of outdoor exposure.

Figure 2G shows the actual cooling performances of our TPCs and indicates that relative to the ambient temperature, a ΔT of 6.3°C was achieved under the solar intensities of 1195 W/m^2 (Figure 4G). At 11:25, a gale caused the temperature drop of ambient and the coating, and there was a minimum with the cooling. Nevertheless, the ΔT was only 1.7°C at night (20:00-5:00). Then, we compared it to the atmospheric temperature and found that the temperature of the inside was over 8.4°C lower than the outside ambient temperature. In other words, the membrane could cool down to 10.1°C below the atmospheric temperature. The illustration shows the location of the test apparatus which is on the roof of a four-story house (about 15 m above the ground); the environment faces the sun. There are no tall buildings around and some trees blow the test apparatus. Therefore, the device would be fully exposed to sunlight without affecting its ability to emit thermal radiation into the surrounding environment. Under these conditions, the radiative cooling effect of TPCs could be investigated (Figure S3).

Other performances of the TPCs

Mechanical strength, flexibility, ductility, and weather resistance play important roles in the resisting deformation of the structure. We evaluated our TPCs and the results indicated that they have good mechanical strength, flexibility, and certain ductility, which greatly widen the actual use of occasions. A TPC of 3 cm wide and 500 um thickness can easily support a farmar of 500 g (Figure 3A). Also, it can be easily bent 180 degrees (Figure 3B) and slowly stretched to twice over original length (Figure 3C). The TPCs have substrate selectivity. Producing on the glass, the TPCs usually auto-fallen off, but attached well on the substrates of wood, plastic, and unpolished metal (Figure 3D). The R_{solar} and ε_{LWIR} curves of TPCs basically coincide about 14 days insolation placed on the roof (Figure 3E), so that the TPC can achieve continuous cooling and good weather resistance.

Thermoelectric generator coated with TPCs

There are many researches on thermoelectric generator using space cold source, but the reported technologies are either high cost or low output. We fabricated a thermoelectric generator with the anisotropic porous PPC. Pasting the produced TPC on a thermoelectric power generation sheet can achieve independent power generation (Figure 4). The used thermoelectric power generation sheet (SP1848-27145 SA) has a conductivity of ~850 Ω^{-1} cm^{-1}, a thermal conductivity of ~15 × 10^{-3} W cm^{-1}·°C^{-1}, and a thermoelectric of merit of ~2.5 × 10^{-3} W °C^{-1}. The thermoelectric generator was fixed 30 cm above the ground with four foam supports (Figure 4A). The top side of the generator plate was cooled by the TPC and the bottom was coated with bitumen for absorbing external heat. For a suspended thermoelectric power generation sheet, the output voltage was almost zero (Figure 4B). After a TPC was affixed to thermoelectric power generation

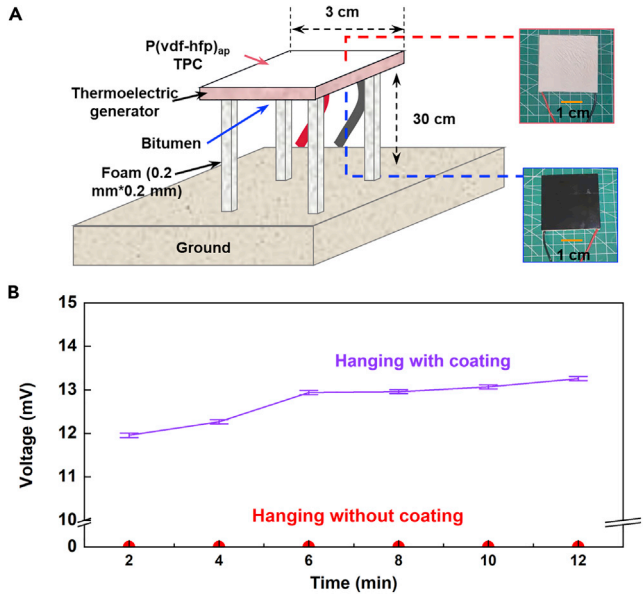

Figure 4. Thermoelectric power generation device and its output voltage

(A) Schematic diagram of module structure of thermoelectric device.

(B) The output voltage of thermoelectric generator with and without the coated TPC. Error bars represent the relative error of the voltmeter (0.5%, Average of three data).

sheet with thermal conductive tape, its output voltage increased to 12 mV at night. Considering that area of the thermoelectric power generation sheet was 4 cm * 4 cm, the power generation voltage can reach 12 mV. This value has exceeded the value of the voltage reported in the previous article about radiative cooling used for thermal power generation (Mu et al., 2019; Xia et al., 2019). Although the output power is low, it has the advantages of low cost, simple process, and scalability. In addition, the thermoelectric generator uses air as the hot source and outer space as the cold source, so it is expected to realize power generation throughout the year. These advantages lead to its great application potential in the field of sensors and Internet of things devices, which require a voltage of no more than 5 V and need little power (Leonov et al., 2007).

DISCUSSION

R_{solar} of the TPCs controlled by NIPS process

The factors affecting the R_{solar} of TPCs mainly depend on their micromorphology such as the aperture sizes and porosities (Dong et al., 2018). Herein, we discuss the influence of polymer concentration and the condensation bath temperature on the aperture sizes and porosities of the TPCs (Figures 5, S4, and S5), because they can affect the double diffusion of non-solvent and solvent to control the shape and size of embedded microspheres (Figures 5A, 5B, and S4A), in turn affecting the R_{solar} and ε_{LWIR} of the coating (Figures 5C, 5D, and S5B). When the polymer concentration was low (13%), the R_{solar} of TPC was more than 89%. Considering the nucleation and growth mechanism, the increased polymer concentration generated a higher polymeric rich phase volume and lower polymeric lean phase volume. Because the polymeric lean phase finally made the pores, the volume of pores reduced with the decrement of the volume of lean phase (Dong et al., 2018; Chen et al., 2021; Cui et al., 2020). As the polymer concentration increased, the diffusion rate of solvent outward and non-solvent inward reduced and the rich phase was gradually occupying the space of lean phase so that scattering ability of TPC was weaker with the porosity and aperture sizes of anisotropic porous decreasing (Figure 5C). When the concentration increased to 20%, the reflectance reduced to 85.6%. In addition, we also analyzed the size distribution of the long and short axes of anisotropic pores (Figure S3) and found that the lengths of l_y and l_z decreased simultaneously and in similar proportions. The anisotropic microporous was retained under different processing conditions. Consequently, the NIPS method can effectively control and regulate the formation of anisotropic pores by the polymer concentration. However, a low concentration of casting solution (e.g. 13%) does not easily form

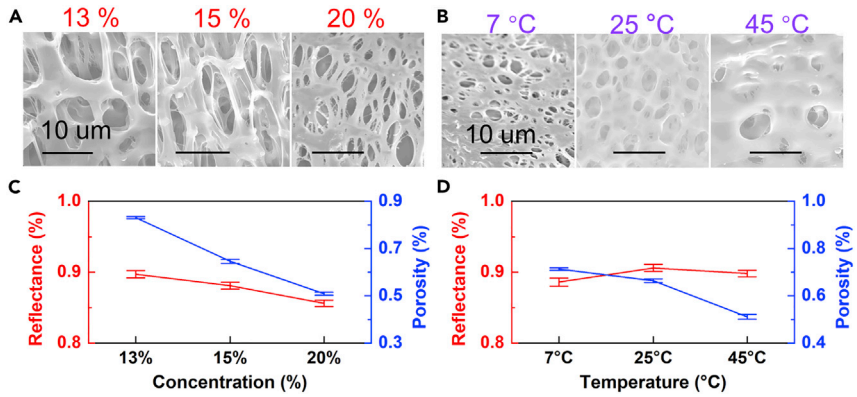

Figure 5. Microstructure and reflectance of TPCs

(A and B) The major and minor axis lengths of the anisotropic pores in cross section views of coatings with different polymer concentrations (13%, 15%, and 20%) and polymer different concentrations (13%, 15%, and 20%).

(C and D) The porosity and the average R_{solar} of the anisotropic pores in cross section views of TPCs obtained at different temperatures of condensed water (7°C, 25°C, and 45°C) and different temperatures of condensed water (7°C, 25°C, and 45°C). Three samples were prepared from each process for performance characterization. Error bars represent standard errors.

a uniform film, and the difference in reflectance between 13% and 15% is only 1.6%. So, we chose 15% as the optimal concentration.

The water temperature of the condensation bath can also affect the R_{solar} by size and number of the anisotropic microporous at keeping polymer concentration (Figures S4B and S5A). When the water was at a lower temperature stage (7°C), the slower mass transfer rate of solvent and non-solvent induced to form small or fragmentary and the R_{solar} was slightly weak. As the water temperature raised to 25°C, the mass transfer rate became fast. Therefore, the lean phase had relatively more time to grow and coalesce. Hence, the micropores in lean phase would expand (Figure 5B). Meanwhile, the polymer gathered, the rich phase coalesced correspondingly. The thickness of the aperture walls and the densification of the coating increased, but the porosity of the coating decreased. Although the porosity of TPC was decreased via the pores number, high R_{solar} of 90.6% was achieved by the increased size (Figure 5D). If the temperature of the condensation bath further increased, despite the pores in lean phase further expanded, the R_{solar} decreased to 89.8% because the rich phase coalesced and even absorbed some micropores. From the comparison of the size distribution of anisotropic pores, we found that l_y and l_z decreased in proportion (Figure S4B), but the range of micropore size change caused by water temperature was smaller than that caused by polymer concentration. In addition, the porosity of the coatings depended on the temperature of the condensation bath and the polymer concentration. In contrast, the variation range of porosity caused by temperature (from 0.713 to 0.511) was weaker than that of polymer concentration (from 0.831 to 0.509). The highest reflectance is at 25°C. In all, both of the polymer concentration and the temperature of the condensation bath have an effect on the R_{solar} by porosity of the TPCs and micromorphology of anisotropic pores. In the end, we finally selected the appropriate process: Mass ratio of 15% polymer concentration and a water temperature of 25°C. The coating thicknesses we tested above were all 400 μm. Reflectance tests of coatings of different thickness are shown in Figure S5C.

Different weather conditions' effect on the cooling effect of TPCs

Generally, the geography and the climate directly affect the radiative cooling performance of TPCs, such as daytime passive radiative cooling power, which is influenced by solar irradiance, humidity, cloud cover, temperature, and surrounding environment. Therefore, we carried out a series of experiments to verify and compare the cooling performance of our TPC in different weather conditions: windy, cloudy, and sunny in Tianjin city (39.26N, 117.06E), and sunny in Panzhihua city, Sichuan province (28.60N, 101.73E), China. The locations of these two cities were shown in Figure S6. As the solar irradiance increased from 428 W/m^2 to 1117 W/m^2, the ambient temperature changed from ~5°C to ~40°C (Figures 6A–6I and S7). Although the humidities were slightly different from weather conditions (24% on the windy day, 30% on the cloudy day, and 16% on the sunny day), the humidities' effect on the cooling of the coating could be ignored compared

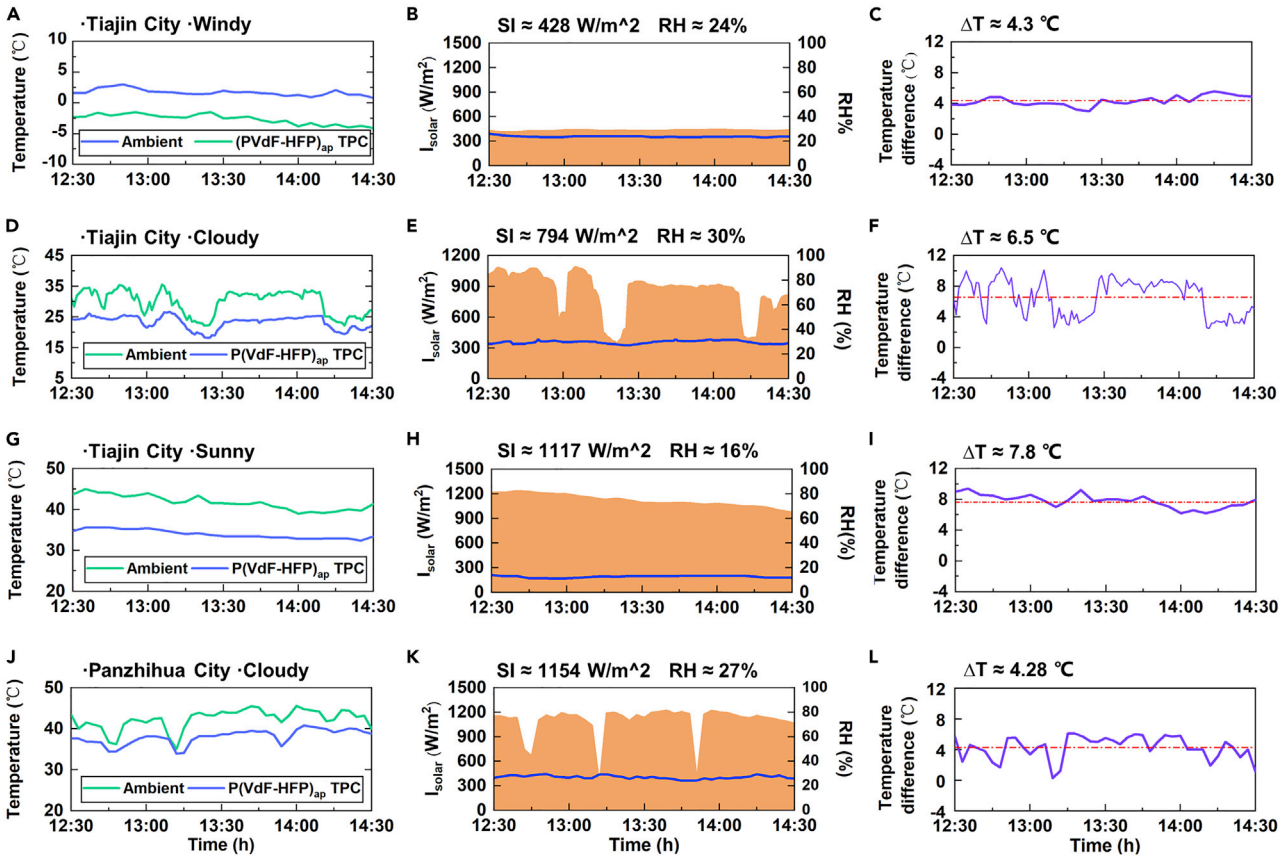

Figure 6. Cooling performance under different weather conditions

(A–C) Temperatures of the ambient air and the TPC, solar irradiance(SI), and relative humidity and the temperature difference of passive daytime radiative cooling on a windy day in Tianjin city.

(D–F) Temperatures of the ambient air and the TPC, Solar irradiance, and relative humidity and the temperature difference of passive daytime radiative cooling on a cloudy day in Tianjin city.

(G–I) Temperatures of the ambient air and the TPC, Solar irradiance, and relative humidity and the temperature difference of passive daytime radiative cooling on a sunny day in Tianjin city.

(J–L) Temperatures of the ambient air and the TPC, Solar irradiance, and relative humidity and the temperature difference of passive daytime radiative cooling on a cloudy day in Panzhihua city.

to the solar irradiance and ambient temperature. The ΔT of the three weather conditions was 4.3°C, 6.5°C, and 7.8°C, respectively, in Tianjin City. The ΔT of 4.28°C was also achieved in Panzhihua, Sichuan, under a weather condition with a high solar irradiance of 1154 W/m^2, a humidity of 27%, and an ambient temperature of 38°C. In Figure 6A–6L and S8, we found that when the solar irradiance reduced due to cloud cover, both the temperatures of the TPCs and ambient fell, but the air dropped more. However, the TPCs with high R_{solar} absorbed little heat from the sun, and the coating's temperature did not change dramatically. This resulted in a smaller calculated cooling temperature difference. The time at the decrease of ΔT in Figures 4F and 4L corresponds to the time at the reduction of solar irradiance in Figures 6E–6K. By comparing Figures 6A–6I, the TPC could achieve cooling temperatures of over 4°C under various weather conditions of noontime. The fundamental reason was that the coating had characteristics of high R_{solar} and high ε_{LWIR}.

NIPS approach extension for specific applications

Based on the difference rate of displacement between solvent and non-solvent, varieties of solvents can be applied to fabricate PPCs for specific applications with NIPS approach (Figure 7A). When DMSO (NMP) was selected as the solvent, the coating was strongly reflective of sunlight, yet the transmittance of visible light was obviously better than others when using acetone as solvent. The PPCs with DMSO (NMP) as solvent could be used in scenes that require both natural lighting and cooling, the PPCs with acetone as solvent

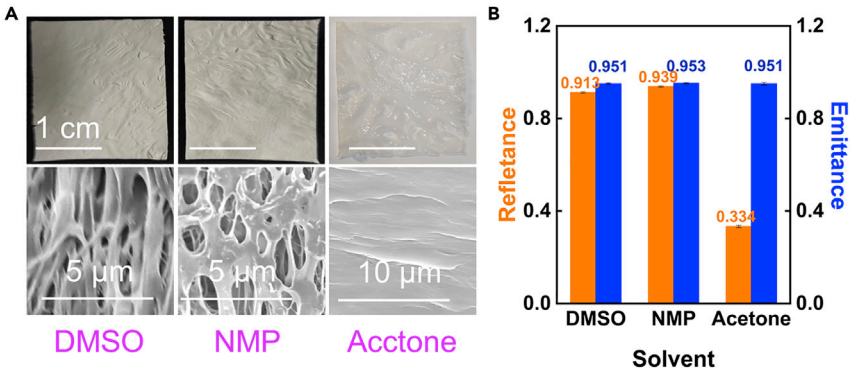

Figure 7. Compatibility of several of solvent

(A) Physical images of PPCs prepared with DMAC, NMP, and acetone and their SEM images.

(B) Rsolar and εLWIR of the PPCs prepared with DMAC, NMP, and acetone. Error bars indicate the uncertainty in measurement. The results are average of three measurements. Error bars represent standard errors.

could be directly covered in the place where was needed for no lighting but cooling. Special to note was that the cross-section SEM images of the PPCs using DMSO and NMP as solvent still showed anisotropic pores, which made the reflectance of these two coatings reach 0.913 and 0.939, respectively (Figure 7B). However, the PPCs with acetone as solvent tended to form a dense structure because acetone and water were mutually soluble in any proportion and the double diffusion rate of solvent and non-solvent was faster. The emittances of these three coatings using DMSO, NMP, and acetone were basically the same (0.951, 0.919, and 0.950).

Limitations of the study

Air temperatures were measured at outside air temperature stations with a temperature sensor, which was directly exposed to the sun. But exposure to the sun did not affect atmospheric temperature measurements because the structure of the station was designed to be applied directly to the refraction of sunlight. A thermocouple for measuring inside air temperature was not exposed to sunlight. For uniform standards, we finally chose to use the outside air temperature as the reference temperature for judging the radiative cooling performance of the coatings. The formation mechanism of anisotropic pores proposed in this work is speculative, based on hydrodynamics and molecular dynamics and has not been investigated experimentally. Pore size was measured with a mercury injection instrument; however, the permeability of the resulting micropores in the coatings was poor, thus resulting in underestimation of the pore size, in comparison to those observed in the SEM image. Thus, to estimate the pore size, we measured the major and minor axes of their ellipsoid shape (values shown in Figure S4). Pore sizes and porosities are dependent on the concentration of P(VdF-HFP), the types of solvents, the condensation bath temperature, the resting time, etc. Here, we discuss the influence of polymer concentration and condensing bath temperature as the more pertinent parameters. Future studies should consider the rest of the parameters as well.

STAR★METHODS

Detailed methods are provided in the online version of this paper and include the following:

- KEY RESOURCES TABLE
- RESOURCE AVAILABILITY
  - Lead contact
  - Materials availability
  - Data and code availability
- METHOD DETAILS
  - Fabrication of TPCs
  - Optical characterizations
  - Porosity characterization
  - Scattering cross section and emittance calculations
- QUANTIFICATION AND STATISTICAL ANALYSIS

SUPPLEMENTAL INFORMATION

Supplemental information can be found online at https://doi.org/10.1016/j.isci.2022.104126.

ACKNOWLEDGMENTS

We appreciate the financial support provided for this research by the Natural Science Foundation of Hebei province of China (F2020202015).

AUTHOR CONTRIBUTIONS

J.Z., Z.A., and X.Z. conceived the concept and designed the research. A.Z. and Z.A. conducted the experiments. Y.G. and Y.D. conducted the FDTD simulations. X.Z. created the schematics. J.Z. and Z.A. wrote the manuscript. All authors including G.C. discussed the results and commented on the manuscript.

DECLARATION OF INTERESTS

The authors declare no competing interests.

Received: December 21, 2021
Revised: February 10, 2022
Accepted: March 17, 2022
Published: April 15, 2022

REFERENCES

Bormashenko, Y., Pogreb, R., Stanevsky, O., and Bormashenko, E. (2004). Vibrational spectrum of PVDF and its interpretation. Polym. Test. *23*, 791–796. https://doi.org/10.1016/j.polymertesting.2004.04.001.

Chen, M., Pang, D., Mandal, J., Chen, X., Yan, H., He, Y., Yu, N., and Yang, Y. (2021). Designing mesoporous photonic structures for high-performance passive daytime radiative cooling. Nano Lett. *21*, 1412–1418. https://doi.org/10.1021/acs.nanolett.0c04241.

Cui, Z., Pan, J., Wang, Z., Frappa, M., Drioli, E., and Macedonio, F. (2020). Hyflon/PVDF membranes prepared by NIPS and TIPS: comparison in MD performance. Sep. Purif. Technol. *247*, 116992. https://doi.org/10.1016/j.seppur.2020.116992.

Dong, X., Al-Jumaily, A., and Escobar, I.C. (2018). Investigation of the use of a bio-derived solvent for non-solvent-Induced phase separation (NIPS) fabrication of polysulfone membranes. Membranes *8*, 23. https://doi.org/10.3390/membranes8020023.

Gentle, A.R., and Smith, G.B. (2015). A subambient open roof surface under the mid-summer sun. Adv. Sci. *2*, 1500119. https://doi.org/10.1002/advs.201500119.

Goldstein, E.A., Raman, A.P., and Fan, S. (2017). Sub-ambient non-evaporative fluid cooling with the sky. Nat. Energy *2*, 17143. https://doi.org/10.1038/nenergy.2017.143.

Kim, M., Kim, G., Kim, J., Lee, D., Lee, S., Kwon, J., and Han, H. (2017). New continuous process developed for synthesizing sponge-type polyimide membrane and its pore size control method via non-solvent induced phase separation (NIPS). Micropor. Mesopor. Mat. *242*, 166–172. https://doi.org/10.1016/j.micromeso.2017.01.013.

Kim, H., McSherry, S., Brown, B., and Lenert, A. (2020). Selectively enhancing solar scattering for direct radiative cooling through control of polymer nanofiber morphology. ACS Appl. Mater. Inter. *12*, 43553–43559. https://doi.org/10.1021/acsami.0c09374.

Kort-Kamp, W.J.M., Kramadhati, S., Azad, A.K., Reiten, M.T., and Dalvit, D.A.R. (2018). Passive radiative "thermostat" enabled by phase-change photonic nanostructures. ACS Photon. *5*, 4554–4560. https://doi.org/10.1021/acsphotonics.8b01026.

Kou, J.-L., Jurado, Z., Chen, Z., Fan, S., and Minnich, A.J. (2017). Daytime radiative cooling using near-black infrared emitters. ACS Photon. *4*, 626–630. https://doi.org/10.1021/acsphotonics.6b00991.

Leonov, V., Torfs, T., Fiorini, P., and Van Hoof, C. (2007). Thermoelectric converters of numan warmth for self-powered wireless sensor nodes. IEEE Sens. J. *7*, 650–657. https://doi.org/10.1109/jsen.2007.894917.

Leroy, A., Bhatia, B., Kelsall, C.C., Castillejo-Cuberos, A., Di Capua, M.H., Zhao, L., Zhang, L., Guzman, A.M., and Wang, E.N. (2019). High-performance subambient radiative cooling enabled by optically selective and thermally insulating polyethylene aerogel. Adv. Sci. *5*, eaat948. https://doi.org/10.1126/sciadv.aat9480.

Li, X., Fang, X., Pang, R., Li, J., Sun, X., Shen, J., Han, W., and Wang, L. (2014). Self-assembly of TiO2 nanoparticles around the pores of PES ultrafiltration membrane for mitigating organic fouling. J. Membr. Sci. *467*, 226–235. https://doi.org/10.1016/j.memsci.2014.05.036.

Li, T., Zhai, Y., He, S., Gan, W., Wei, Z., Heidarinejad, M., Dalgo, D., Mi, R., Zhao, X., Song, J., et al. (2019). A radiative cooling structural material. Science *364*, 760–763. https://doi.org/10.1126/science.aau9101.

Li, D., Liu, X., Li, W., Lin, Z., Zhu, B., Li, Z., Li, J., Li, B., Fan, S., Xie, J., et al. (2021). Scalable and hierarchically designed polymer film as a selective thermal emitter for high-performance all-day radiative cooling. Nat. Nanotechnol. *16*, 153–158. https://doi.org/10.1038/s41565-020-00800-4.

Liu, J., Lu, X.-L., and Wu, C.-R. (2013). Effect of annealing conditions on crystallization behavior and mechanical properties of NIPS poly(vinylidene fluoride) hollow fiber membranes. J. Appl. Polym. Sci. *129*, 1417–1425. https://doi.org/10.1002/app.38845.

Liu, C., Sun, Y., Chen, Z., and Zhang, S. (2019). From ultrafiltration to nanofiltration: nanofiltration membrane fabricated by a combined process of chemical crosslinking and thermal annealing. Sep. Purif. Technol. *212*, 465–473. https://doi.org/10.1016/j.seppur.2018.11.041.

Liu, S., Chu, Y., Tang, C., He, S., and Wu, C. (2020). High-performance chlorinated polyvinyl chloride ultrafiltration membranes prepared by compound additives regulated non-solvent induced phase separation. J. Membr. Sci. *612*, 118434. https://doi.org/10.1016/j.memsci.2020.118434.

Luque-Alled, J.M., Abdel-Karim, A., Alberto, M., Leaper, S., Perez-Page, M., Huang, K., Vijayaraghavan, A., El-Kalliny, A.S., Holmes, S.M., and Gorgoj, P. (2020). Polyethersulfone membranes: from ultrafiltration to nanofiltration via the incorporation of APTS functionalized-graphene oxide. Sep. Purif. Technol. *230*, 115836. https://doi.org/10.1016/j.seppur.2019.115836.

Mandal, J., Fu, Y., Overvig, A.C., Jia, M., Sun, K., Shi, N.N., Zhou, H., Xiao, X., Yu, N., and Yang, Y. (2018). Hierarchically porous polymer coatings for highly efficient passive daytime radiative cooling. Science *362*, 315–318. https://doi.org/10.1126/science.aat9513.

Munday, J.N. (2019). Tackling climate change through radiative cooling. Joule *3*, 2057–2060. https://doi.org/10.1016/j.joule.2019.07.010.

Mu, E., Wu, Z., Wu, Z., Chen, X., Liu, Y., Fu, X., and Hu, Z. (2019). A novel self-powering ultrathin TEG device based on micro/nano emitter for radiative cooling. Nano Energy *55*, 494–500. https://doi.org/10.1016/j.nanoen.2018.10.057.

Peng, Y., Chen, J., Song, A.Y., Catrysse, P.B., Hsu, P.-C., Cai, L., Liu, B., Zhu, Y., Zhou, G., Wu, D.S., et al. (2018). Nanoporous polyethylene microfibres for large-scale radiative cooling fabric. Nat. Sustain. *1*, 105–112. https://doi.org/10.1038/s41893-018-0023-2.

Raman, A.P., Anoma, M.A., Zhu, L., Rephaeli, E., and Fan, S. (2014). Passive radiative cooling below ambient air temperature under direct sunlight. Nature *515*, 540–544. https://doi.org/10.1038/nature13883.

Sim, L.N., Majid, S.R., and Arof, A.K. (2012). FTIR studies of PEMA/PVdF-HFP blend polymer electrolyte system incorporated with LiCF3SO3 salt. Vib. Spectrosc. *58*, 57–66. https://doi.org/10.1016/j.vibspec.2011.11.005.

Ulaganathan, M., and Rajendran, S. (2010). Effect of different salts on PVAc/PVdF-co-HFP based polymer blend electrolytes. J. Appl. Polym. Sci. *118*, 646–651. https://doi.org/10.1002/app.32404.

Wang, X., Liu, X., Li, Z., Zhang, H., Yang, Z., Zhou, H., and Fan, T. (2020). Scalable flexible hybrid membranes with photonic structures for daytime radiative cooling. Adv. Funct. Mater. *30*, 1907562. https://doi.org/10.1002/adfm.201907562.

Wang, T., Wu, Y., Shi, L., Hu, X., Chen, M., and Wu, L. (2021). A structural polymer for highly efficient all-day passive radiative cooling. Nat. Commun. *12*, 365. https://doi.org/10.1038/s41467-020-20646-7.

Xia, Z., Zhang, Z., Meng, Z., Ding, L., and Yu, Z. (2019). Thermoelectric generator using space cold source. ACS Appl. Mater. Inter. *11*, 33941–33945. https://doi.org/10.1021/acsami.9b10981.

Xiang, B., Zhang, R., Luo, Y., Zhang, S., Xu, L., Min, H., Tang, S., and Meng, X. (2021). 3D porous polymer film with designed pore architecture and auto-deposited SiO2 for highly efficient passive radiative cooling. Nano Energy *81*, 105600. https://doi.org/10.1016/j.nanoen.2020.105600.

Yampolskii, Y. (2012). Polymeric gas separation membranes. Macromolecules *45*, 3298–3311. https://doi.org/10.1021/ma300213b.

Yang, M., Zou, W., Guo, J., Qian, Z., Luo, H., Yang, S., Zhao, N., Pattelli, L., Xu, J., and Wiersma, D.S. (2020). Bioinspired "skin" with cooperative thermo-optical effect for daytime radiative cooling. ACS Appl. Mater. Inter. *12*, 25286–25293. https://doi.org/10.1021/acsami.0c03897.

Zhang, X.A., Yu, S., Xu, B., Li, M., Peng, Z., Wang, Y., Deng, S., Wu, X., Wu, Z., Ouyang, M., et al. (2019). Dynamic gating of infrared radiation in a textile. Science *363*, 619–623. https://doi.org/10.1126/science.aau1217.

Zhang, H., Ly, K.C.S., Liu, X., Chen, Z., Yan, M., Wu, Z., Wang, X., Zheng, Y., Zhou, H., and Fan, T. (2020). Biologically inspired flexible photonic films for efficient passive radiative cooling. P. Natl. Acad. Sci. U S A. *117*, 14657–14666. https://doi.org/10.1073/pnas.2001802117.

Zhai, Y., Ma, Y., David, S.N., Zhao, D., Lou, R., Tan, G., Yang, R., and Yin, X. (2017). Scalable-manufactured randomized glass-polymer hybrid metamaterial for daytime radiative cooling. Science *355*, 1062–1066. https://doi.org/10.1126/science.aai7899.

Zhou, K., Li, W., Patel, B.B., Tao, R., Chang, Y., Fan, S., Diao, Y., and Cai, L. (2021). Three-dimensional printable nanoporous polymer matrix composites for daytime radiative cooling. Nano Lett. *21*, 1493–1499. https://doi.org/10.1021/acs.nanolett.0c04810.

STAR★METHODS

KEY RESOURCES TABLE

REAGENT or RESOURCE	SOURCE	IDENTIFIER
Chemicals, peptides, and recombinant proteins		
P(VdF-HFP)	Kynar Flex	2801-00
N,N-Dimethylformamide	aladdin	D112004
Dimethyl sulfoxide	aladdin	D103272
Acetone	Tianjin Fengchuan Chemical Reagent Co., Ltd	N/A
Deionized Water	aladdin	W119424
Other		
Spectrophotometer	SHIMADZU	UV-3600
INVENIO Fourier Transform Infrared (FT-IR)	BURKER	INVENIO
Mercury Porosimeter	Micromeritics	Auto Pore IV 9510
Scanning Electron Microscope	JEOL	JSM-7610F
K Thermocouple	SMART SENSOR	AS877
Portable-meteorological Station	Shandong Renke Control technology Co., Ltd	N/A
Thermoelectric Power Generation Sheet	Shenzhen Xinquan Technology Co., Ltd	TGM-287-1.4-1.5

RESOURCE AVAILABILITY

Lead contact

Further information and requests for resources and reagents should be directed to and will be fulfilled by the lead contact, Jiliang Zhu (jlzhu@hebut.edu.cn).

Materials availability

This study did not generate new unique reagents.

Data and code availability

- All data reported in this paper will be shared by the lead contact upon request.
- This paper does not report original code.
- Any additional information required to reanalyze the data reported in this paper is available from the lead contact upon request.

METHOD DETAILS

Fabrication of TPCs

P(VdF-HFP) (PVdF-HFP 2801) from Dongguan Zhanyang polymer materials Co., Ltd was dissolved in N,N-Dimethylformamide (RHWARN), strring for more than 2 h using power magnetic mixer to make a precursor solution with a mass concentration of 15%. The precursor solution was then spin-coated or blade-coated onto different substrates. The wet coatings thickness could be adjusted by changing the height between the scaper and the substrate. Wet coatings thickness gauges could be used during coating to ensure correct thickness. Individual coatings could be detached from smooth surfaces like glass or aluminium. Other substrates such as wood and plastic could be used to make the coatings stick to their surfaces tightly.

In order to make the film produced in the experiment have good uniformity and reproducibility, special attention should be paid to the following operation points during the production:

①The casting solution should be kept in a sealed and dark condition to prevent the solution from volatilizing and the components from self-assembling. ②It is necessary to stop or vacuum the casting solution to remove the air bubbles. Blade coatings should also be avoided in the process of scraping. ③Drying or heat

treatment of the film will cause shrinkage of the pore aperture, so the temperature and time need to be controlled well. We dried coatings for 2 h at 80°C at 0.1 atmosphere.

The polymer solution and solvent are scraped onto the appropriate support and then immersed in the non-solvent of the coagulation bath. Deionized water is used as the condensate. Solvent and non-solvent exchange, liquid-liquid or solid-liquid separation occurs. The structure of the resulting membrane is determined by both mass transfer and phase separation. In order to meet different industrial requirements, different additives or non-solvents are often added to the casting solution, or the structure and performance of the microporous membrane are adjusted by controlling the composition of the solidification bath. Due to the many factors involved in this method and the rich process control methods, the membrane structures prepared are also diverse. In addition, the operating temperature required by NIPS membrane process is generally lower than 80°C, so the energy consumption of membrane production is less.

Optical characterizations

Spectral transmittance of the TPCs was determined separately in the visible to near-infrared (0.3–2.4 μm) and near-infrared to mid-infrared (3–20 mm) wavelength ranges. For the first range, measurement was taken at specific wavelengths from UV-VIS-NIR spectrophotometer (UV-3600, SHIMADZU) with a self-fitting integrating sphere. For the second range, a fourier transform infrared spectrometer (INVENIO R, PIKE) with Mid- Infrared IR Integrating Sphere Accessory was used for measurement. The measurement was 12° downward sample positioning.

Porosity characterization

Porosity was measured by a mercury porosimeter (Micromeritics Auto Pore IV 9510, Narcross).o Imaging and Microscopy.

The mages of samples were taken using smart phone. The scanning electron microscopy was done using a scanning electron microscope (JSM-7610F, JEOL).

Scattering cross section and emittance calculations

The scattering cross section was calculated using the finite difference time domain (FDTD) method. The scattering cross section of micropores was calculated using two-dimensional calculation. The first reason was that limited computer memory was needed to reduce computational load. The second reason was that it had been reported that individual two- dimensional and three-dimensional pores showed similar scattering efficiency in pore radius functions of different wavelengths. For the calculations, spectral refractive indices of P(VdF-HFP) were obtained from the article.

QUANTIFICATION AND STATISTICAL ANALYSIS

In the experiment of the effect of polymer concentration and condensation bath temperature on the pore size and porosity of TPCs, the descriptive statistics method was used for the intra-group comparison, and the average value of each group of data was used for analysis.